科学通报 2021 年 第 66 卷 第 26 期: 3412 ~ 3425
评 述
《中国科学》杂志社
SCIENCE CHINA PRESS

多层结构对镧系掺杂纳米颗粒上转换发光的调控作用

秦昌云, 谢贤彬, 马颖*

华中科技大学材料科学与工程学院, 材料成形与模具技术国家重点实验室, 武汉 430074

* 联系人, E-mail: yingma@hust.edu.cn

2020-12-09 收稿, 2021-02-10 修回, 2021-02-18 接受, 2021-03-11 网络版发表

国家自然科学基金(21673090, 21871099)、湖北省自然科学基金创新群体项目(2019CFA002)和中央高校基本科研业务费(2019kfyXMBZ018)资助

摘要 镧系离子掺杂的上转换纳米颗粒(upconversion nanoparticles, UCNPs)由于具有较大的反斯托克斯位移, 良好的发光与化学稳定性, 长激发态寿命及尖锐的多谱线发射等独特性质, 在生物成像和检测、疾病诊断和治疗、安全防伪以及太阳能电池等多个领域备受关注. 然而传统UCNPs受到发光效率低、浓度猝灭等诸多问题的限制, 实际应用举步维艰. 相比较而言, 通过多层结构设计可以对掺杂离子浓度、上转换能量传递过程等进行更有效的调控, 从而对纳米颗粒的发光性能进行调节与优化, 所以具有多层结构的UCNPs近几年来备受关注. 本文主要综述了多层结构在UCNPs发光性能调控中的主要作用: 多重激发和发光的调节、能量传递调控、实现高浓度掺杂的高效发光以及对寿命的大范围调控, 同时结合一些应用实例展望了多层结构的UCNPs在显示、生物医疗以及安全防伪等多个领域的应用前景.

关键词 上转换纳米颗粒, 多层结构, 能量传递调控, 高效发光, 发光寿命调控

镧系离子掺杂的上转换纳米颗粒(upconversion nanoparticles, UCNPs)是一类典型的纳米发光材料, 由于镧系离子4f电子壳层具有阶梯状能级分布, 可以吸收两个或多个低能光子而发射出高能的光子[1,2]. 这种较大的反斯托克斯位移特性使UCNPs可以应用在安全防伪[3,4]、太阳能捕获[5]、超分辨成像[6]、固态激光器[7]、无背景的生物传感和光触发药物传输[8~10]等多个领域[11~15]. 但目前由于上转换发光效率低, 镧系离子掺杂的UCNPs在各领域的实际应用大受限制, 因此如何进一步提高UCNPs的发光效率一直是该领域亟待解决的问题.

核壳结构(如$NaYF_4$:20%Yb,2%Er@$NaYF_4$)的设计是上转换纳米材料发展过程中的一个里程碑. 与单核纳米颗粒(如$NaYF_4$:Yb,Er; LaF_3:Yb,Er; $NaGdF_4$:Yb,Tm等)相比, 核壳结构能抑制表面配体、缺陷、分子等引起的发光猝灭, 从而显著提高UCNPs的发光强度与发光效率[16], 因此核壳结构自从2007年被成功合成[17~20]后就被广泛研究和应用, 已成为镧系掺杂的UCNPs的主要构筑结构之一[21,22].

近年来, 由于合成方法以及表征技术手段的日益成熟, 多层结构的UCNPs受到越来越多的关注. 因为多层结构的设计不仅可以保留传统核壳结构的优势(抑制表面猝灭), 还能对纳米颗粒的上转换能量传递过程进行调控, 由此带来了许多传统核壳结构难以具备的性能与优势, 不久的将来有望在生物检测与成像等多个领域得到实际应用. 本文将从多重发光调节、能量传递的调控与设计、高效发光以及寿命调控4个方面概括总结多层结构对于镧系掺杂纳米颗粒上转换发光

引用格式: 秦昌云, 谢贤彬, 马颖. 多层结构对镧系掺杂纳米颗粒上转换发光的调控作用. 科学通报, 2021, 66: 3412–3425
Qin C Y, Xie X B, Ma Y. Regulating the upconversion luminescence of lanthanide-doped nanoparticles through multilayered structure (in Chinese). Chin Sci Bull, 2021, 66: 3412–3425, doi: 10.1360/TB-2020-1565

© 2021《中国科学》杂志社

的重要调控作用.

1 多重发光调节

由于一种激活离子的发光颜色比较单一，而多种激活离子共掺必然促进交叉弛豫, 引起浓度猝灭, 多层结构则可以实现不同激活离子的空间分离，可以看作是多种单核或核壳结构的集合. 因此相比于发光性质单一、可调范围有限的传统结构上转换纳米颗粒而言, 多层结构拓宽了发光性能的调控范围，使上转换发光更加可调和丰富多彩, 主要体现在以下两个方面.

1.1 全色发光调节

多层结构为我们提供了一个平台，不仅可以让纳米颗粒的发光性质更丰富(如多激活剂离子发光[23,24]、全色调节[25]、强的宽光谱发射[26,27]等)[28~30]，而且调控手段[25,31~36](温度、功率、掺杂量与掺杂种类、脉冲宽度等)更多元、可控程度更高. 与传统的固定发射颜色的染料或量子点相比，这种可调节发光性质的多层结构纳米晶用于生物标记可以显著提高成像的可靠性和方便性，也大大拓展了这种上转换纳米颗粒在显示、生物成像、安全防伪、疾病诊断与治疗等多个领域的应用.

最近几年，人们不再局限于通过多个激活离子分别掺杂到不同壳层实现多层结构的全色发光调节，开始探索更加多元化的发光调节方式. 例如, 2015年刘小刚团队[37]报道了一种对脉冲宽度敏感的六方相$NaYF_4$多层结构上转换纳米颗粒，基于对非稳态上转换过程中能量传递的动态控制: 在808 nm连续光激发时, 通过Nd→Yb→Tm的能量传递, 三光子吸收使Tm^{3+}的4f壳层电子发生$^3H_6\rightarrow{}^1G_4$的能级跃迁(图1(a))，重新回到基态时发射出470 nm的蓝色光. 在980 nm的脉冲光激发下则发生Yb→Ho的能量转移，但脉冲宽度的长短控制着Ho^{3+}电子在不同能级之间的跃迁过程，若脉冲时间短, Ho^{3+}吸收双光子发生$^5I_8\rightarrow{}^5I_6\rightarrow{}^5F_4/{}^5S_2$的能级跃迁(图1(a))，然后从激发态回到基态发射出541 nm的绿光；对于长脉冲激发, Ho^{3+}中间能级$^5I_6$会与Ce^{3+}发生交叉弛豫然后延迟失活到$^5I_7$能级，再吸收一个激发光子能量由$^5I_7$能级跃迁到$^5F_5$能级(图1(a))，对应于646 nm的红光发射. 通过两种激光以及脉冲宽度的调控实现了这种多层结构UCNPs的全色调控(图1(b)). 同年，张忠平课题组[38]合成了23 nm的$NaGdF_4$:Yb/Tm/Er@$NaGdF_4$:Eu@$NaYF_4$六方相多层结构纳米颗粒, 将分别发射红、绿、蓝光的3种离子(Eu^{3+}、Er^{3+}、Tm^{3+})掺杂到同一个纳米颗粒中，发现3种颜色的发光强度随激光功率密度的增大而增大, 但增大速率不同(Eu^{3+}的红光发射>Tm^{3+}的蓝光发射>Er^{3+}的绿光发射)，导致3种颜色在总发射强度中的比例发生变化(图1(c))，由此通过激发功率的调节不仅可以实现整个可见光波段的发光，而且实现了极强的白光发射. 2017年, 邵起越团队[35]在研究温度调控多色发光时, 为了提高UCNPs的多色调节能力, 合成了28.5 nm的六方相$NaGdF_4$:Yb/Tm@$NaGdF_4$@$NaGdF_4$:Yb/Ho@$NaGdF_4$:Yb(Tm@Gd@Ho@Yb)多层结构. 内核Tm^{3+}的蓝色发光被外面壳层屏蔽而不受温度影响；而Ho^{3+}的红光与绿光发射由于受到表面吸附水分子带来的发光猝灭，随着温度升高水分子的减少, Ho^{3+}发光逐渐增强(图1(d)). 纳米颗粒整体发光颜色因此发生由蓝色→白色→绿色的渐变. 上述这些发光颜色可调的UCNPs在安全防伪、温度传感等多个领域有着巨大的应用前景. 例如，应用在平板显示(图1(e))[38]与立体显示(图1(f))[39]领域，可以获得高分辨率和清晰度的彩色图像.

1.2 相互独立的多波段激发发光

利用多层结构除了可调节上转换发射颜色外，还可通过多种敏化剂离子掺杂和分布调控，在单个纳米颗粒上实现较强的宽光谱吸收[40]或多个激发波段独立吸收与发光. 最常见的便是980和808 nm的双波段激发发光[41~43]，如果掺杂Ce^{3+}还可以吸收高能波段光(254 nm), 同时实现上转换与下转换的多波段激发独立发光[25,44]. 这种互不干扰的多波段激发纳米颗粒可以更充分利用各个激发波段的独特优势，比如在安全防伪方面可以提供更多的检测维度[42].

2016年，张凡课题组[45]构建了85 nm的六方相$NaGdF_4$:Yb,Er@$NaYF_4$:Yb@$NaGdF_4$:Yb,Nd@ $NaYF_4$@$NaGdF_4$:Yb,Tm@$NaYF_4$(C-S1-S2-S3-S4-S5, C为核; S为壳)多层结构(图2(a)). 通过中间$NaYF_4$层完全隔绝两组敏化-激活离子对的相互作用，在单纳米颗粒可以呈现出两组独立的上转换发光: 980 nm激发时, 敏化剂Yb^{3+}吸收能量后传递给激活剂离子Tm^{3+}, Tm^{3+}通过5光子吸收过程实现紫外/蓝光发射(图2(b)，S4壳层). 796 nm激发下, 先由Nd^{3+}吸收激发光能量, 然后发生Nd→Yb→Er的能量传递，Er^{3+}的双光子吸收实现明亮的绿光/红光发射(图2(b)，C-S1-S2壳层). 这种多激发调控机制随后得到广泛研究和应用. 2018年，常钰磊团队[46]合成了

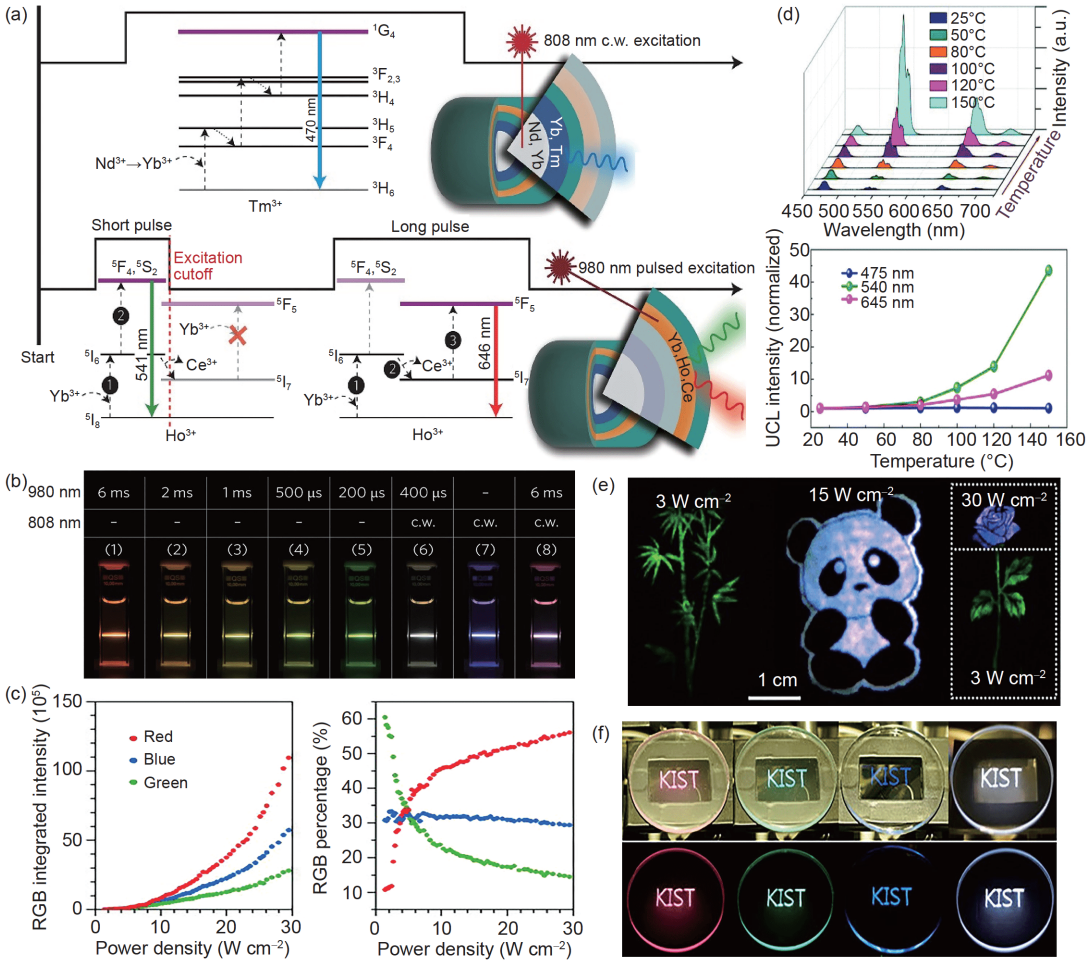


图 1 多层结构发光的全色调节及其在显示领域的应用. (a) 非稳态上转换机理; (b) 脉冲宽度调节实现全色发光[37]; (c) 功率全色调节机理[38]; (d) 温度调节机理[35]; (e) 平板显示[38]; (f) 透明立体显示[39]

Figure 1 Multi-color tuning and applications in display for multilayered UCNPs. (a) The non-steady-state upconversion mechanisms; (b) luminescence photographs showing full-color emission modulated by pulse width[37]; (c) the mechanisms of full-color emission regulated by power[38]; (d) the mechanisms of full-color emission regulated by temperature[35]; (e) application in flat-panel display[38]; (f) application in transparent volumetric display[39]

40 nm的六方相$NaErF_4$@$NaYF_4$@$NaYbF_4$:0.5% Tm@$NaYF_4$多层结构纳米颗粒, 尽管没有Nd^{3+}作为敏化剂, 也可以实现800和980 nm分别激发Er^{3+}和Tm^{3+}的上转换发光. 2019年, 张勇课题组[47]构建的哑铃形(27 nm×60 nm)六方相$NaYbF_4$:Er/Tm@$NaYF_4$:Yb@-$NaNdF_4$:Yb多层结构, 由于能量传递路径不同, 可以在980和808 nm激发下分别实现Er^{3+}的红光和绿光发射. 这种相互独立的多波段激发发光在生物医疗领域的应用价值非凡: 利用C-S1-S2-S3-S4-S5多层结构在980 nm激发时产生的光热效应以及紫外/蓝光发射引起的光异构化可协同触发化疗药物的释放, 而796 nm激发带来的绿光/红光发射可单独应用于光动力治疗(photodynamic therapy, PDT)(图2(c)). 并且实验结果也表明这种多层结构的UCNPs在两种波段的近红外光共同激发下癌细胞杀死率较796 nm单独激发下高出很多. $NaErF_4$@$NaYF_4$@$NaYbF_4$:0.5%Tm@$NaYF_4$多层结构的光控上转换发光可以实现实时监测与成像的高效PDT过程(图2(d)). 而通过对$NaYbF_4$:Er/Tm@$NaYF_4$:Yb@$NaNdF_4$:Yb纳米颗粒的激发调控可以对同一细胞类型的多个离子通道进行有序、按需和可编程的激活(图2(e)), 这一特性对于多通道的生物过程调控是非常有利的.

2 借助能量迁移调控能量传递路径

传统的上转换发光机理包括双光子吸收(two-

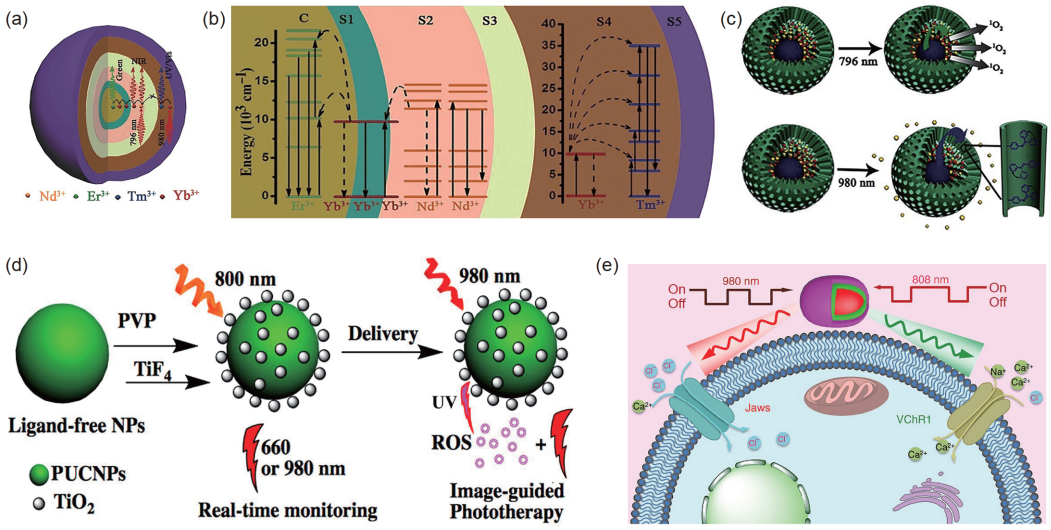


图 2 (网络版彩色)多层结构的多波段激发发光及其在生物医药领域的应用. (a, b) C-S1-S2-S3-S4-S5多层结构及发光机理; (c) C-S1-S2-S3-S4-S5多层结构纳米颗粒光动力治疗与化疗的应用原理[45]; (d) 光控上转换纳米颗粒(PUCNPs)应用于实时监测与影像导航的光动力治疗(reactive oxygen species, ROS, 活性氧)[46]; (e) 可编程激活细胞离子通道蛋白Jaws和VChR1的原理图[47]

Figure 2 (Color online) Orthogonal excitations-emissions of multilayered UCNPs and their applications in biological and medical domains. (a, b) The structure and luminescence mechanism of C-S1-S2-S3-S4-S5 UCNPs; (c) schematic of PDT and chemotherapy of C-S1-S2-S3-S4-S5 UCNPs[45]; (d) the schematic diagram of real-time monitoring and image-guided phototherapy using PUCNPs@TiO_2 (reactive oxygen species, ROS)[46]; (e) schematic of programmable activation of ion channel proteins Jaws and VChR1[47]

photon absorption, TPA)、二次谐波的产生(second-harmonic generation, SHG)、激发态吸收(excited state absorption, ESA)、能量传递上转换(energy transfer upconversion, ETU)和光子雪崩(photon avalanche, PA). 其中ETU是稀土离子掺杂纳米材料上转换发光的最有效方式, 最早由Auzel[48]于1966年在块体材料的研究中发现. 这是一种敏化剂-激活剂耦合的体系, 即由敏化剂离子吸收激发光能量然后传递给激活剂离子, 借助激活剂离子的多个长寿命的中间能级促进后续的光子吸收和能量转移, 从而实现较大反斯托克斯位移的上转换发光, 如图1(a)和2(b)所示. 这种上转换发光机理的能量传递过程清晰, 但高效的ETU过程通常只局限于Yb-Er/Ho/Tm敏化剂-激活剂体系.

能量迁移介导上转换(energy migration-mediated upconversion, EMU)是一种新型的上转换能量传递机理, 在传统ETU过程的基础上, 借助Gd^{3+}之间的能量迁移过程来实现敏化剂-激活剂之间的间接能量传递. 这种能量迁移发生在同一种离子之间, 因此具有本征的吸收发射谱重合[49], 这一特征使得能量迁移过程极易发生并且可以长距离能量传输, 实现了多种激活剂离子的高效上转换发光, 大大拓宽了上转换材料的范围, 因此EMU机理自2011年提出[50]后备受关注.

多层结构构建是调控Gd^{3+}介导能量迁移上转换发光的常规手段. 2012年, 刘小刚团队[51]最早构筑了尺寸接近20 nm的六方相$NaGdF_4$:Yb/Tm@$NaGdF_4$:A@$NaYF_4$多层结构纳米颗粒, 其能量传递机理如图3(a)所示: Tm^{3+}吸收5个光子能量由$^3H_6$能级跃迁到$^1I_6$能级, 然后将能量传递给Gd^{3+}, 即发生Tm^{3+}($^1I_6$)→Gd^{3+}($^6P_{7/2}$)的能量传递, 借助基质中Gd^{3+}的$^6P_{7/2}$能级将能量迁移到激活剂离子A(A=Sm, Tb, Eu, Dy)的激发态能级(Sm^{3+}的$^4G_{5/2}$能级, Tb^{3+}的$^5D_3$和$^5D_4$能级, Eu^{3+}的$^5D_3$、$^5D_2$、$^5D_1$和$^5D_0$能级, Dy^{3+}的$^4F_{9/2}$能级), 实现其发光. 并且通过惰性层抑制表面猝灭进一步提高激活剂离子A的发光效率, 实现极低激活剂离子A掺杂浓度(低至1%)下的高效可控上转换发光(图3(b)). 这一研究开启了利用多层结构实现过渡金属与多种稀土离子高效EMU发光的大门[13,39,52,53], 例如, 2017与2018年先后报道通过这种结构实现Ce^{3+}与Nd^{3+}的上转换发光[54,55]. 此外, 利用多层结构还可以对Gd^{3+}介导的能量迁移过程进行调控, 由此提高能量传递效率或者调控纳米颗粒的发光性能. 如前所述, 借助$NaGdF_4$基质可以实现长距离的能量迁移和传递[56], 但能量传递效率随$NaGdF_4$的厚度增加而显著降低, 当惰性层$NaYF_4$存在时尤为严重[50,51], 1.7 nm的$NaYF_4$惰性层就基本可以阻

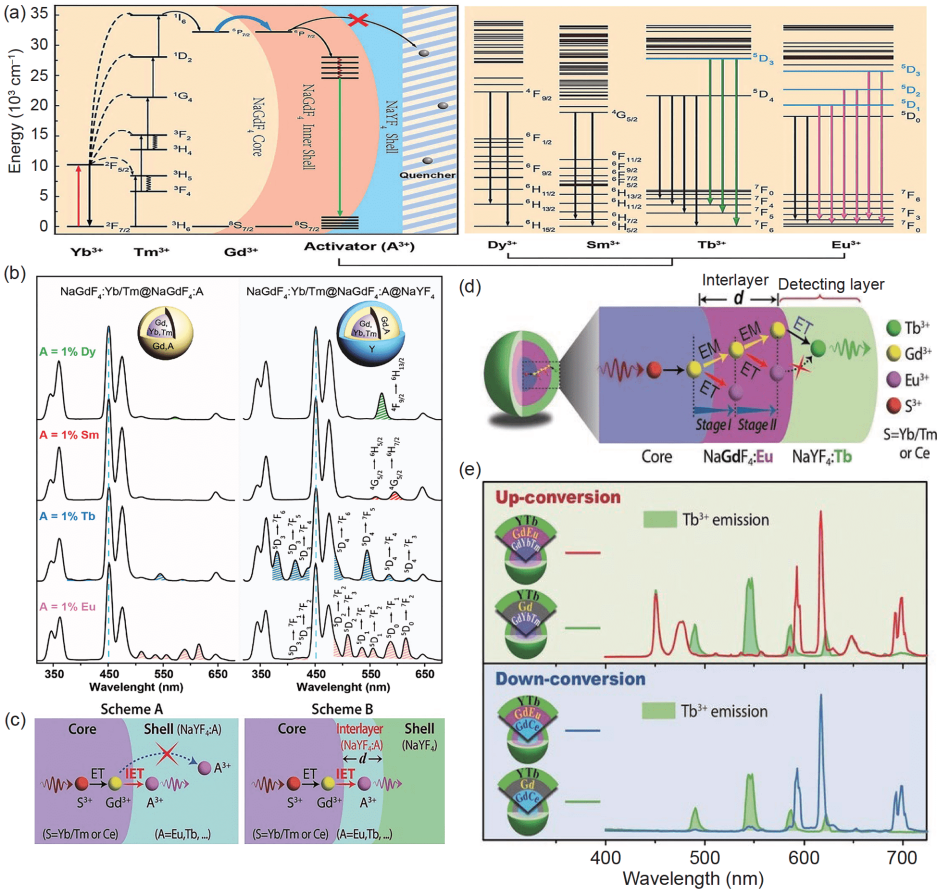


图 3 (网络版彩色)利用多层结构对能量迁移介导上转换的调控. (a, b) $NaGdF_4$:Yb/Tm@$NaGdF_4$:A@$NaYF_4$纳米颗粒的能量传递机理与上转换发光光谱[51]; (c) $NaYbF_4$:Tm/Gd@$NaYF_4$:A与$NaYbF_4$:Tm/Gd@$NaYF_4$:A@$NaYF_4$纳米颗粒的Gd^{3+}介导界面能量传输[57]; (d) 调控Gd^{3+}的能量迁移(EM)与能量传递(ET)过程; (e) Eu^{3+}与Tb^{3+}的上下转换发光[57]

Figure 3 (Color online) Regulating energy migration-mediated upconversion via multilayered structure. (a, b) The energy migration upconversion mechanism and upconversion luminescence (UCL) spectra of $NaGdF_4$:Yb/Tm@$NaGdF_4$:A@$NaYF_4$ UCNPs[51]; (c) the Gd^{3+}-mediated interfacial energy transfer (IET) for $NaYbF_4$:Tm/Gd@$NaYF_4$:A and $NaYbF_4$:Tm/Gd@$NaYF_4$:A@$NaYF_4$ UCNPs[57]; (d) regulating the Gd^{3+}-mediated energy migration (EM) and energy transfer (ET) process; (e) the upconversion and downconversion luminescence spectrum of Eu^{3+} and Tb^{3+}[57]

断Gd^{3+}到Tb^{3+}的能量传递. 张勤远课题组[57]通过比较含有惰性基质壳层的核壳结构和三层结构的EMU发光(图3(c)), 发现EMU过程主要是由界面能量传递主导, 高效能量传递主要局限于距离核/壳界面1.5 nm之内. 当纳米颗粒内部涉及多种能量传递路径时, 例如在$NaGdF_4$:Yb/Tm@$NaGdF_4$:Eu@$NaYF_4$:Tb多层结构中, 存在着两种竞争的能量传递路径(图3(d)): Gd→Eu的界面能量传递与Gd→Gd→Tb的能量迁移传递, 分别对应着Eu^{3+}与Tb^{3+}的发光, 通过中间层厚度的调节, 可以有效调控两种能量传递过程, 从而精确调控两种离子的发光比例, 当中间层厚度大于4 nm时, Gd→Gd→Tb的能量传递被完全抑制, 实现Eu^{3+}的选择性发光(图3(e)).

3 提高发光效率

众所周知, 限制镧系掺杂的上转换纳米颗粒发光效率的主要原因有两个: 第一是猝灭中心, 即能量通过掺杂离子迁移到颗粒晶体缺陷、表面配体、水分子等引起的能量非辐射损耗现象, 传统的核壳结构(如$NaYF_4$:20%Yb,2%Er@$NaYF_4$)便是通过抑制能量向表面猝灭中心迁移从而显著提高发光效率; 第二是浓度猝灭, 即掺杂离子浓度过高使得敏化剂和激活剂等离子之间的间距小于临界距离(2~6 nm)[58], 掺杂离子之间的交叉弛豫导致能量损耗. 由于稀土离子对近红外激发光的本征吸收截面较传统发光材料和有机染料等小几个数量级, 浓度猝灭的限制使得UCNPs的发光难

以满足生物成像和检测等领域的实际需求. 而多层结构的设计不仅能抑制猝灭中心带来的发光猝灭, 而且还能抑制浓度猝灭, 实现敏化剂离子对近红外激发光吸收的最大化[59], 同时提高其发光效率, 从而带来发光强度的显著提高.

3.1 抑制缺陷猝灭

晶体缺陷作为一种发光猝灭中心, 往往是在三维空间随机分布的, 核壳结构的设计只能抑制晶体表面猝灭中心引起的发光猝灭, 而多层结构的构筑在抑制表面猝灭的基础上还能最大程度地抑制晶体内部缺陷猝灭, 从而带来发光强度的大幅提高, 以满足实际应用的需求.

2014年, Summers团队[60]提出一种"δ掺杂"多层结构: 约46 nm的六方相$NaYF_4$@$NaYF_4$:Yb,Er@$NaYF_4$纳米颗粒. 他们通过理论计算和实验证明, 相比于三维球体(发光核)和二维平面分布, 将共掺杂离子限制在二维球面区域(中间壳层)时, 掺杂离子与三维空间随机分布的缺陷间能量传递几率最低(图4(a)), 即缺陷猝灭最小化, 因此更多的能量可以通过敏化剂Yb^{3+}转移到激活剂Er^{3+}实现发光的显著提高(图4(b)). 2016年, 王锋课题组[61]进一步证实这种结构中敏化剂离子的浓度可以进一步提高, 即中间壳层可以直接采用$NaYbF_4$基质, 制备得到的38 nm六方相$NaYF_4$@$NaYbF_4$:Tm@$NaYF_4$多层结构(图4(c))在减少缺陷猝灭的同时提高了Yb^{3+}吸收的能量向Tm^{3+}的转移几率, 大大提高了上转换发光强度, 尤其是深紫外波段的发射强度获得两个数量级的提升(图4(d)), 有望应用于近红外激发的深紫外激光器中. 随后, 这种多层结构(尤其是对于高浓度掺杂体系)被广泛采用[62~67], 例如2018年Steven Chu课题组[68]就合成了29 nm的六方相$NaYF_4$@$NaYb_{1-x}F_4$:Er_x@$NaYF_4$多层结构, 实现整体发光强度2个数量级的提高(图4(e)), 在低至8 W/cm^2的功率下检测到其单粒子发光, 作为细胞内单分子检测探针的潜力巨大. 还有许多研究者对这种结构作了进一步改进[69], 将原结构中的惰性核与惰性层改换成掺杂敏化剂离子的活性核与活性层. 例如, 文献[70]报道的30 nm×17 nm的棒状六方相$NaGdF_4$:Yb@$NaYF_4$:Yb/Er@$NaGdF_4$:Yb(图4(f)), 抑制体内缺陷猝灭的同时显著提高纳米颗粒对激发光的吸收(活性核与活性壳层都可以吸收), 实现发光强度的大幅提升.

3.2 抑制浓度猝灭

如前所述, 当敏化剂和激活剂离子掺杂浓度较高时, 掺杂离子间会发生交叉弛豫(浓度猝灭). 尤其是敏化剂离子能级也呈现多阶梯分布时, 激活剂和敏化剂离子间的能量回传极为严重, 大大地限制了掺杂浓度与能量传递效率. 多层结构的设计可以精确控制掺杂离子的分布与含量, 实现掺杂量的最佳化, 还可以选择

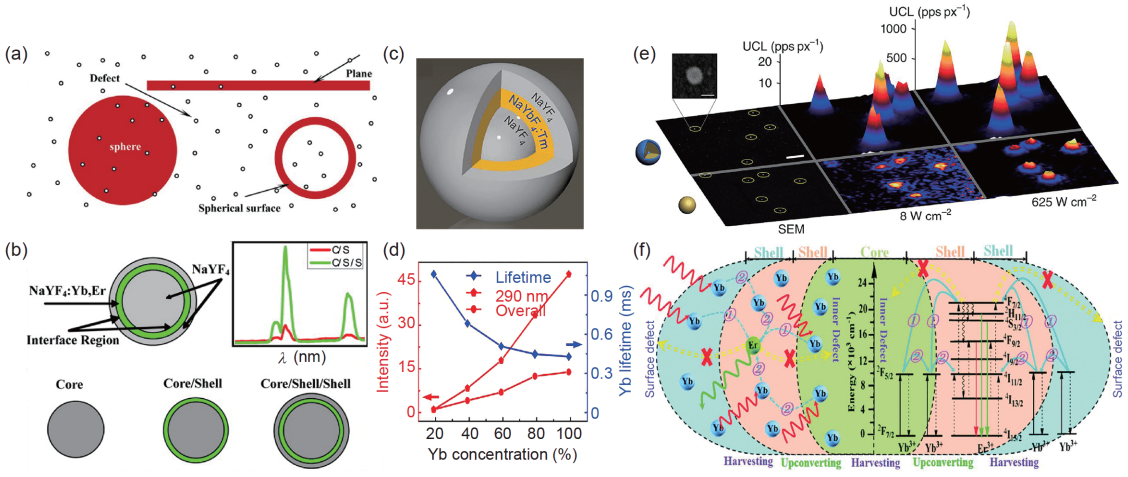


图 4 (网络版彩色)多层结构抑制缺陷猝灭. (a) 球面、平面、球体的缺陷态密度示意图[60]; (b) $NaYF_4$@$NaYF_4$:Yb,Er@$NaYF_4$纳米颗粒的结构与发光[60]; (c, d) $NaYF_4$@$NaYbF_4$:Tm@$NaYF_4$多层结构及发光强度[61]; (e) $NaYF_4$@$NaYb_{1-x}F_4$:Er_x@$NaYF_4$纳米颗粒的上转换发光(UCL)强度[68]; (f) $NaGdF_4$:Yb@$NaYF_4$:Yb/Er@$NaGdF_4$:Yb多层结构能量传递示意图[70]

Figure 4 (Color online) Efficient suppression of energy loss caused by defects in multilayered structures. (a) Defects density of spherical surface, plane, and sphere[60]; (b) structure and UCL intensity of $NaYF_4$@$NaYF_4$:Yb,Er@$NaYF_4$ UCNPs[60]; (c, d) structure and UCL intensity of $NaYF_4$@$NaYbF_4$:Tm@$NaYF_4$ UCNPs[61]; (e) UCL intensity of $NaYF_4$@$NaYb_{1-x}F_4$:Er_x@$NaYF_4$ UCNPs[68]; (f) schematic illustration of the energy transfer process in $NaGdF_4$:Yb@$NaYF_4$:Yb/Er@$NaGdF_4$:Yb UCNPs[70]

性地分隔掺杂敏化剂和激活剂离子于不同壳层，从而有效抑制能量回传或交叉弛豫，大大提高能量传递效率，实现高效上转换发光. 近年来，通过这种方式对浓度猝灭的抑制作用，使多层结构UCNPs的敏化剂离子掺杂浓度可以逐渐从20%趋于极限100%[61,71,72](即采用$NaYbF_4$/$LiYbF_4$等基质)，激活剂离子的掺杂浓度也显著提高，如本课题组[73]采用多层结构将Er掺杂浓度从2%提高到10%, Tm掺杂浓度从1%提高到8%.

Nd^{3+}对于800 nm激发光有较大的吸收截面，因而Nd^{3+}常用作800 nm近红外激发的敏化剂. 但是Nd^{3+}复杂的4f电子能级分布，使得激活剂离子和Nd^{3+}之间存在严重的能量回传，大大限制了Nd^{3+}敏化的UCNPs发光效率. 2014年，本课题组[74]采用16 nm的六方相$NaYF_4$:Yb,Er@$NaYF_4$:Yb@$NaNdF_4$:Yb三层结构，通过中间过渡层抑制Er^{3+}与Nd^{3+}间的能量回传(图5(a))，采用$NaNdF_4$为基质的同时优化Yb的掺杂量与分布(敏化剂层Nd^{3+}的含量达到90%)，使其800 nm近红外光激发下的上转换发光较传统Nd/Yb/Er共掺核壳结构(Nd^{3+}的最佳掺杂浓度值大约为1%)和$NaYF_4$:Yb,Er@$NaYF_4$:Nd核壳纳米颗粒分别提高了100和8倍. 这种利用多层结构将敏化剂与激活剂分隔在不同壳层的方法为抑制交叉弛豫和提高上转换发光强度开辟了新思路，现已被大家广泛采用[40,75~80]. 由于Nd^{3+}敏化通常需要经Yb^{3+}将能量传递给激活剂离子，因此上述结构中不同壳层Yb的含量也对能量在Yb亚晶格的传递效率有重要影响. 2015年，戴宏杰团队[81]制备了粒径50 nm左右的六方相$NaYF_4$:2%Er,α%Yb@$NaYF_4$:β%Yb@$NaNdF_4$:γ%Yb(@α:β:γ)多层结构(图5(b))，他们发现掺杂比例α、β、γ改变时，Yb亚晶格的能量传递效率存在明显差异. 因此通过优化纳米颗粒内部Yb的掺杂量与分布，可以实现能量在Yb亚晶格的最高效传递，大幅提高发光强度(图5(c))且相应的量子产率可以提高10倍以上.

Yb^{3+}作为更常用的敏化剂离子，与Nd^{3+}不同的是，其能级结构单一，因此激活剂离子和Yb^{3+}之间的交叉弛豫问题长期被人们忽视. 近几年，敏化剂Yb^{3+}与激活剂离子间的交叉弛豫或能量回传也逐渐受到重视. Berry团队[82]对$NaYF_4$:Yb,Er@$NaYF_4$中上转换发光动力学的理论分析表明，近邻Er^{3+}/Yb^{3+}对Er^{3+}发光有明显猝灭作用，并且这些Er^{3+}还会成为Yb^{3+}激发的猝灭中心. 2019年，Ki-Bum Lee团队[83]发现在57 nm的六方相$NaYF_4$:Yb@$NaYF_4$:Er@$NaYF_4$:Yb(Yb@Er@Yb)纳米颗粒中，Yb^{3+}和Er^{3+}的空间分隔可以有效消除Yb^{3+}-Er^{3+}之

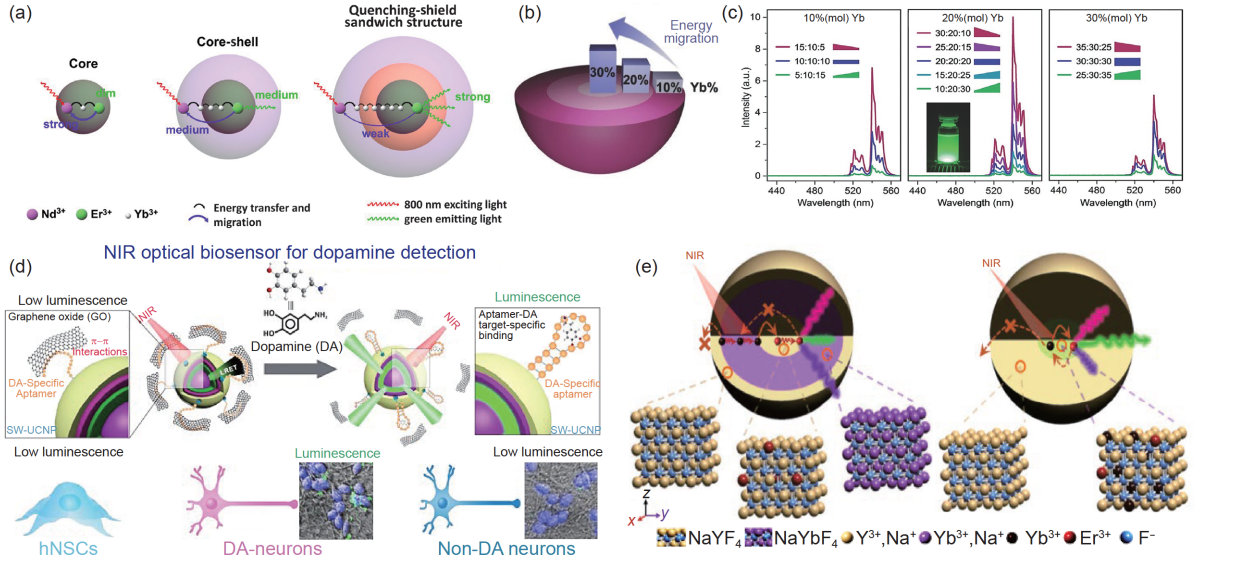


图 5 (网络版彩色)多层结构抑制交叉弛豫. (a) $NaYF_4$:Yb,Er@$NaYF_4$:Yb@$NaNdF_4$:Yb多层结构抑制Nd-Er的能量回传示意图[74]; (b, c) @α:β:γ多层结构及不同Yb掺杂浓度的发光光谱[81]; (d) Yb@Er@Yb三层结构上转换纳米颗粒("sandwich" structured UCNP, SW-UCNP)在人神经干细胞(human neural stem cells, hNSCs)中对多巴胺(DA)的检测(近红外, NIR)[83]; (e) $NaYF_4$:Er@$NaYbF_4$@$NaYF_4$多层结构抑制Yb-Er交叉弛豫示意图[73]

Figure 5 (Color online) Efficient suppression of cross-relaxation by multilayered UCNPs. (a) Schematic of suppressing cross-relaxation between Nd-Er in $NaYF_4$:Yb,Er@$NaYF_4$:Yb@$NaNdF_4$:Yb multilayered structure[74]; (b, c) structure of @α:β:γ UCNPs and UCL spectra of @α:β:γ UCNPs with different Yb^{3+} doping concentrations[81]; (d) the application in live cell dopamine (DA) sensing in human neural stem cell-derived neural interfaces of Yb@Er@Yb UCNPs (near-infrared, NIR)[83]; (e) schematic of suppressing cross-relaxation between Yb-Er in $NaYF_4$:Er@$NaYbF_4$@$NaYF_4$ UCNPs[73]

间的交叉弛豫, 实现发光强度的明显提升, 因此制成的生物传感器可以对神经干细胞释放的多巴胺进行超敏检测(图5(d)). 这与本课题组[73]最近报道的$NaYF_4$:10% Er@$NaYbF_4$@$NaYF_4$三层结构(32 nm左右, 立方相和六方相)不谋而合, 通过Yb-Er高效界面能量传递, 在抑制Yb-Er之间交叉弛豫作用的同时, 有效抑制了表面猝灭(图5(e)), 可以实现$NaYbF_4$层敏化(即100% Yb浓度)、10%Er或8%Tm掺杂浓度下的高效上转换发光, 使得Er^{3+}的多光子发射(407 nm)较传统核壳结构提高了100多倍, 发光量子产率因此大幅提升, UCNPs向着多个领域的实际应用迈进了一大步.

4 发光寿命调节及其应用

荧光成像技术可以通过荧光探针标记等对细胞和组织中的特定分子和蛋白质的位置和迁移过程等进行实时观察, 在生物医学领域应用广泛. 传统的荧光成像主要通过采集荧光发射强度信号成像, 因荧光强度不仅受生物组织(骨头、脂肪、皮肤、肌肉、体液等)吸收与散射的影响, 而且受荧光探针浓度、光漂白、激发和检测效率的影响, 难以精确定量. 与之相比, 荧光寿命主要取决于荧光探针的种类和周围微环境, 基本不受上述因素影响, 因此比荧光发射强度更容易进行定量, 并且对微环境的改变也更为敏感, 空间分辨率高, 尤其是组织深层的成像方面更有优势, 目前广泛应用于生物功能、病理和疾病诊疗研究中[84]. 荧光寿命成像技术主要有时域和频域调制两大类方法, 其中时域调制法相对于频域调制具有更高的成像速度和时间分辨率等优点, 因此在现代医学技术中备受关注. 时间相关单光子计数(time correlated single photon counting, TCSPC)是目前时域调制荧光寿命成像技术中应用最广泛、技术最成熟的一种[85]. 随着固体超快激光技术的进步, 结合多光子激发荧光显微技术、共焦显微技术等, 荧光寿命的超快检测成为现实, 因此近年来基于TCSPC的寿命成像技术被广泛采用[86], 尤其是在生物成像方面有望取代传统荧光成像技术.

镧系掺杂纳米颗粒可以被近红外光激发, 对生物组织损伤小且穿透深度深, 同时荧光寿命长(远长于生物组织的自荧光寿命), 信噪比高, 作为寿命成像生物探针具有得天独厚的优势. 多层结构的设计, 不仅可以实现其发光颜色的大范围调控, 更让我们可以对纳米颗粒的荧光寿命实现大范围(微秒到毫秒级)精确调控, 丰富了时域代码, 因而多层结构的镧系纳米颗粒在多级防伪[52]、安全编码、信息存储以及生物成像和检测等方面(尤其是活体生物组织深层检测)的应用价值远远高于传统核壳结构.

2017年, 刘小刚团队[87]利用多层结构纳米颗粒融合了长寿命的Mn^{2+}和相对短寿命的Tm^{3+}的上转换发射(图6(a), (b)), 将两种寿命组成二进制时间码, 不仅可以突破传统上转换纳米颗粒信息存储容量低或安全防伪复杂性不足的瓶颈, 而且不需要设置时间门控来分离和解码安全数据. 2018年, 张凡课题组[88]设计了20 nm的六方相$NaGdF_4$@$NaGdF_4$:Yb,Er@$NaYF_4$:Yb@-$NaNdF_4$:Yb多层结构(图6(c)), 实现了在两个维度上的发光寿命调控. 一方面, 增加能量传递层的厚度, 延长了从吸收到发射的平均过程, 即延长了寿命. 另一方面, 对于某一固定厚度的能量传递层, 即在Yb^{3+}亚晶格储存的激发光子能量相同时, Er^{3+}浓度的增加加速了储存能量向发射光的转换, 缩短寿命. 由此可实现单一发射峰的发光寿命范围在跨越3个数量级内精确调控(图6(d)), 在活体生物深层组织(深达8 mm)寿命成像检测时完全不受影响(而荧光强度成像的信噪比明显降低). 他们利用这种多层结构的纳米颗粒进行寿命多重成像可以成功识别活体老鼠的肿瘤亚型. 2020年, 陈冠英课题组[89,90]也先后报道了$NaYF_4$:Yb/Er@$NaYbF_4$@$NaYF_4$@$NaYF_4$:Nd(32~48 nm)与$NaYF_4$@$NaYbF_4$@$NaYF_4$:Yb/Tm@$NaYF_4$(26~41 nm)两种六方相多层结构纳米颗粒, 分别实现了3~10 ms和78~2157 μs寿命的精确调控, 成功应用于活体生物多重寿命成像(图6(e))与多级防伪图案(图6(f)). 此外, 多层结构的UCNPs在多重编码的应用上还可以结合发光颜色调控, 利用颜色/寿命的二进制编码使其多重编码能力较传统结构利用颜色/强度进行编码的能力提高几个数量级以上[91,92], 大大拓宽了光学多重编码材料的范围.

5 结论与展望

本文总结了利用多层结构对UCNPs上转换发光性能的多重调控, 以及这些具有优异发光性能的多层结构纳米颗粒在彩色显示、生物医疗、安全防伪等领域的潜在应用. 第一, 多层结构使掺杂离子种类以及壳层设计方面具有更多的自由度, 因此相比于传统核壳结构, 具有多层结构的UCNPs不论是在吸收(多波段独立)还是发射(全色、全光谱)波段都更多元, 因此可以用于多功能和复杂体系的应用, 大幅提高实用性. 第二, 多

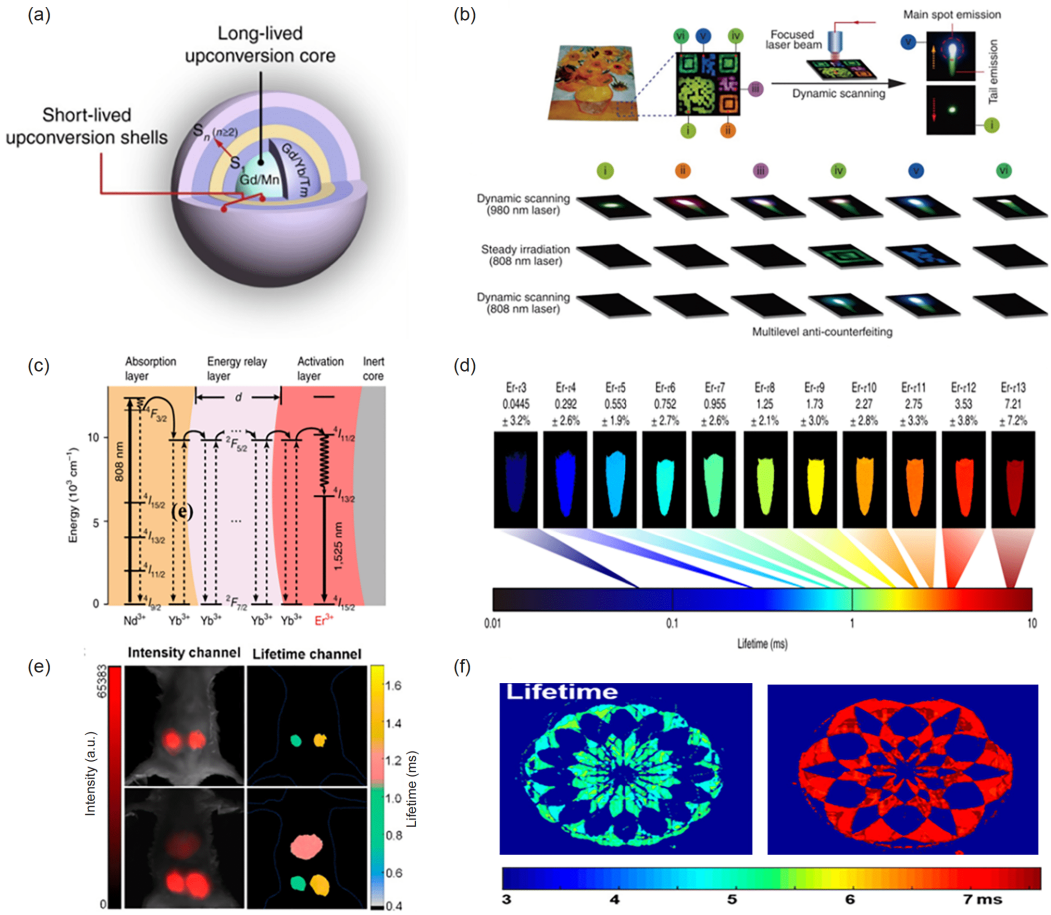


图 6 (网络版彩色)多层结构对寿命的调节及其应用. (a, b) Mn/Tm双寿命体系的多层结构与多级防伪应用[87]; (c, d) $NaGdF_4$@$NaGdF_4$:Yb,Er@$NaYF_4$:Yb@$NaNdF_4$:Yb多层结构能量迁移机制与寿命调控[88]; (e, f) 活体生物的多重寿命成像[89]和寿命编码的多级防伪图案[90]

Figure 6 (Color online) Lifetime tuning of multilayered UCNPs and its applications. (a, b) The structure and multilevel anti-counterfeiting application of Mn/Tm dual-lifetime system[87]; (c, d) the energy migration mechanism and lifetime tunability of $NaGdF_4$@$NaGdF_4$:Yb,Er@$NaYF_4$:Yb@$NaNdF_4$:Yb UCNPs[88]; (e, f) temporal multiplexed *in vivo* upconversion imaging[89] and lifetime-encoding patterns for multilevel anti-counterfeiting[90]

层结构还能对上转换的能量传递过程进行调控, 尤其是涉及能量迁移介导的上转换发光过程, 不仅能够实现多种激活剂离子(Dy^{3+}、Sm^{3+}、Tb^{3+}、Eu^{3+}、Ce^{3+}、Mn^{2+})的高效上转换发光, 还能对Gd^{3+}的能量迁移过程进行优化与调控. 第三, 相比于传统的核壳结构, 多层结构既能有效抑制表面猝灭, 还能显著抑制晶体内部缺陷猝灭与交叉弛豫, 实现高浓度掺杂的UCNPs的高效发光. 除了发光波段和强度以外, 多层结构还可以从多个维度调控纳米颗粒的发光寿命, 对寿命多重编码以及信息储存等领域意义非凡.

总之, 多层结构的镧系掺杂纳米颗粒为上转换发光性能和能量传递调控带来了更多机遇和可能性, 尤其是在医疗、信息存储、多重成像、生物检测与安全防伪等领域具有很好的应用前景. 但是多层结构的UCNPs依然存在诸多挑战: 首先, 镧系离子的本征吸收截面小, 多层结构虽能提高发光效率以及掺杂浓度, 但整体发光强度还是比较低, 所以将来可以进行多层结构的有机染料敏化、光子晶体构建以及等离子增强方面的研究; 另外, 目前多层结构纳米颗粒的合成存在着费时费力、壳层厚度可控性和重复性差等问题, 开展更简便普适的可控合成方法尤为重要. 2018年, 格拉斯哥大学的Leroy Cronin团队[93]通过将清洗/混合/搅拌/加料/抽真空/结晶/加热/冷却/过滤/转移等一系列化学实验步骤编写成为一套计算机语言, 并通过一套特定的计算机程序控制机器执行复杂的有机合成过程, 成功合成了多种复杂药物, 其产率及纯度完全不低于、甚至高于人工合成产物. 这样的合成方法不仅完全排除了人为因素对于合成的影响, 而且将复杂的合成过程

转换为特定的数字代码，可以发布、版本化且兼容性极佳，从而大大提高了复杂分子合成可重复性和可靠性. 化学合成数字化的发展趋势[94,95]，也让我们看到人工智能合成复杂多层结构的可能和更好的可控性.

参考文献

1 Liu Y, Lu Y, Yang X, et al. Amplified stimulated emission in upconversion nanoparticles for super-resolution nanoscopy. Nature, 2017, 543: 229–233

2 Zhou B, Shi B, Jin D, et al. Controlling upconversion nanocrystals for emerging applications. Nat Nanotechnol, 2015, 10: 924–936

3 You M, Zhong J, Hong Y, et al. Inkjet printing of upconversion nanoparticles for anti-counterfeit applications. Nanoscale, 2015, 7: 4423–4431

4 Sun T, Xu B, Chen B, et al. Anti-counterfeiting patterns encrypted with multi-mode luminescent nanotaggants. Nanoscale, 2017, 9: 2701–2705

5 Chan E M. Combinatorial approaches for developing upconverting nanomaterials: High-throughput screening, modeling, and applications. Chem Soc Rev, 2015, 44: 1653–1679

6 Chen C, Wang F, Wen S, et al. Multi-photon near-infrared emission saturation nanoscopy using upconversion nanoparticles. Nat Commun, 2018, 9: 3290

7 Fernandez-Bravo A, Yao K, Barnard E S, et al. Continuous-wave upconverting nanoparticle microlasers. Nat Nanotechnol, 2018, 13: 572–577

8 Wilhelm S. Perspectives for upconverting nanoparticles. ACS Nano, 2017, 11: 10644–10653

9 Liu B, Chen Y, Li C, et al. Poly(acrylic acid) modification of Nd^{3+}-sensitized upconversion nanophosphors for highly efficient UCL imaging and pH-responsive drug delivery. Adv Funct Mater, 2015, 25: 4717–4729

10 Dai Y, Bi H, Deng X, et al. 808 nm near-infrared light controlled dual-drug release and cancer therapy *in vivo* by upconversion mesoporous silica nanostructures. J Mater Chem B, 2017, 5: 2086–2095

11 Huang H, Huang F, Lin L, et al. Perceiving linear-velocity by multiphoton upconversion. ACS Appl Mater Interfaces, 2019, 11: 46379–46385

12 Ao Y, Zeng K, Yu B, et al. An upconversion nanoparticle enables near infrared-optogenetic manipulation of the *Caenorhabditis elegans* motor circuit. ACS Nano, 2019, 13: 3373–3386

13 Huang C H, Park Y I, Lin H Y, et al. Compact and filter-free luminescence biosensor for mobile *in vitro* diagnoses. ACS Nano, 2019, 13: 11698–11706

14 Zhang X, Ai F, Sun T, et al. Multimodal upconversion nanoplatform with a mitochondria-targeted property for improved photodynamic therapy of cancer cells. Inorg Chem, 2016, 55: 3872–3880

15 Ai F, Ju Q, Zhang X, et al. A core-shell-shell nanoplatform upconverting near-infrared light at 808 nm for luminescence imaging and photodynamic therapy of cancer. Sci Rep, 2015, 5: 10785

16 Wang F, Wang J, Liu X. Direct evidence of a surface quenching effect on size-dependent luminescence of upconversion nanoparticles. Angew Chem Int Ed, 2010, 49: 7456–7460

17 Yi G S, Chow G M. Water-soluble $NaYF_4$:Yb,Er(Tm)/$NaYF_4$/polymer core/shell/shell nanoparticles with significant enhancement of upconversion fluorescence. Chem Mater, 2007, 19: 341–343

18 Mai H X, Zhang Y W, Sun L D, et al. Highly efficient multicolor up-conversion emissions and their mechanisms of monodisperse $NaYF_4$:Yb,Er core and core/shell-structured nanocrystals. J Phys Chem C, 2007, 111: 13721–13729

19 Wang Y, Qin W P, Zhang J S, et al. Synthesis and upconversion luminescence of LaF_3:Yb^{3+}, Er^{3+}/SiO_2 core/shell microcrystals. J Rare Earths, 2007, 25: 605–608

20 Boyer J C, Gagnon J, Cuccia L A, et al. Synthesis, characterization, and spectroscopy of $NaGdF_4$:Ce^{3+},Tb^{3+}/$NaYF_4$ core/shell nanoparticles. Chem Mater, 2007, 19: 3358–3360

21 Johnson N J J, He S, Diao S, et al. Direct evidence for coupled surface and concentration quenching dynamics in lanthanide-doped nanocrystals. J Am Chem Soc, 2017, 139: 3275–3282

22 Pilch A, Würth C, Kaiser M, et al. Shaping luminescent properties of Yb^{3+} and Ho^{3+} co-doped upconverting core-shell β-$NaYF_4$ nanoparticles by dopant distribution and spacing. Small, 2017, 13: 1701635

23 Huang H, Chen J, Liu Y, et al. Lanthanide-doped core@multishell nanoarchitectures: Multimodal excitable upconverting/downshifting luminescence and high-level anti-counterfeiting. Small, 2020, 16: 2000708

24 Wu M, Yan L, Wang T, et al. Controlling red color-based multicolor upconversion through selective photon blocking. Adv Funct Mater, 2019, 29: 1804160

25 Yin X, Wang H, Tian Y, et al. Three primary color emissions from single multilayered nanocrystals. Nanoscale, 2018, 10: 9673–9678

26 Shao W, Chen G, Kuzmin A, et al. Tunable narrow band emissions from dye-sensitized core/shell/shell nanocrystals in the second near-infrared biological window. J Am Chem Soc, 2016, 138: 16192–16195

27 Skripka A, Marin R, Benayas A, et al. Covering the optical spectrum through collective rare-earth doping of $NaGdF_4$ nanoparticles: 806 and 980 nm excitation routes. Phys Chem Chem Phys, 2017, 19: 11825–11834

28 Cao C, Zhou X, Xue M, et al. Dual near-infrared-emissive luminescent nanoprobes for ratiometric luminescent monitoring of ClO^- in living organisms. ACS Appl Mater Interfaces, 2019, 11: 15298–15305

29 Li J, Zhu X, Xue M, et al. Nd^{3+}-sensitized upconversion nanostructure as a dual-channel emitting optical probe for near infrared-to-near infrared fingerprint imaging. Inorg Chem, 2016, 55: 10278–10283

30 Kim S Y, Jeong J S, Mkhoyan K A, et al. Direct observation of the core/double-shell architecture of intense dual-mode luminescent tetragonal bipyramidal nanophosphors. Nanoscale, 2016, 8: 10049–10058

31 Shang Y, Han Q, Hao S, et al. Dual-mode upconversion nanoprobe enables broad-range thermometry from cryogenic to room temperature. ACS Appl Mater Interfaces, 2019, 11: 42455–42461

32 Lei L, Dai X, Cheng Y, et al. Dual-mode color tuning based on upconversion core/triple-shell nanostructure. J Mater Chem C, 2019, 7: 3342–3350

33 Serge Correales Y E, Hazra C, Ullah S, et al. Precisely tailored shell thickness and Ln^{3+} content to produce multicolor emission from Nd^{3+}-sensitized Gd^{3+}-based core/shell/shell UCNPs through bi-directional energy transfer. Nanoscale Adv, 2019, 1: 1936–1947

34 Hao S, Chen G, Yang C, et al. Nd^{3+}-sensitized multicolor upconversion luminescence from a sandwiched core/shell/shell nanostructure. Nanoscale, 2017, 9: 10633–10638

35 Shao Q, Zhang G, Ouyang L, et al. Emission color tuning of core/shell upconversion nanoparticles through modulation of laser power or temperature. Nanoscale, 2017, 9: 12132–12141

36 Cortelletti P, Skripka A, Facciotti C, et al. Tuning the sensitivity of lanthanide-activated NIR nanothermometers in the biological windows. Nanoscale, 2018, 10: 2568–2576

37 Deng R, Qin F, Chen R, et al. Temporal full-colour tuning through non-steady-state upconversion. Nat Nanotechnol, 2015, 10: 237–242

38 Zhang C, Yang L, Zhao J, et al. White-light emission from an integrated upconversion nanostructure: Toward multicolor displays modulated by laser power. Angew Chem Int Ed, 2015, 54: 11531–11535

39 Shin J, Kyhm J H, Hong A R, et al. Multicolor tunable upconversion luminescence from sensitized seed-mediated grown $LiGdF_4$:Yb,Tm-based core/triple-shell nanophosphors for transparent displays. Chem Mater, 2018, 30: 8457–8464

40 Shao W, Chen G, Ohulchanskyy T Y, et al. Lanthanide-doped fluoride core/multishell nanoparticles for broadband upconversion of infrared light. Adv Opt Mater, 2015, 3: 575–582

41 Wen H, Zhu H, Chen X, et al. Upconverting near-infrared light through energy management in core-shell-shell nanoparticles. Angew Chem Int Ed, 2013, 52: 13419–13423

42 Lei Z, Ling X, Mei Q, et al. An excitation navigating energy migration of lanthanide ions in upconversion nanoparticles. Adv Mater, 2020, 32: e1906225

43 Ma Q, Wang J, Li Z, et al. Near-infrared-light-mediated high-throughput information encryption based on the inkjet printing of upconversion nanoparticles. Inorg Chem Front, 2017, 4: 1166–1172

44 Lin H, Cheng Z, Xu D, et al. A novel upconversion core-multishell nanoplatform for a highly efficient photoswitch. J Mater Chem C, 2020, 8: 3483–3490

45 Li X, Guo Z, Zhao T, et al. Filtration shell mediated power density independent orthogonal excitations-emissions upconversion luminescence. Angew Chem Int Ed, 2016, 55: 2464–2469

46 Zuo J, Tu L, Li Q, et al. Near infrared light sensitive ultraviolet-blue nanophotoswitch for imaging-guided “off-on” therapy. ACS Nano, 2018, 12: 3217–3225

47 Mei Q, Bansal A, Jayakumar M K G, et al. Manipulating energy migration within single lanthanide activator for switchable upconversion emissions towards bidirectional photoactivation. Nat Commun, 2019, 10: 4416

48 Auzel F. Upconversion and anti-stokes processes with f and d ions in solids. Chem Rev, 2004, 104: 139–174

49 Zhou B, Huang J, Yan L, et al. Probing energy migration through precise control of interfacial energy transfer in nanostructure. Adv Mater, 2019, 31: e1806308

50 Wang F, Deng R, Wang J, et al. Tuning upconversion through energy migration in core-shell nanoparticles. Nat Mater, 2011, 10: 968–973

51 Su Q, Han S, Xie X, et al. The effect of surface coating on energy migration-mediated upconversion. J Am Chem Soc, 2012, 134: 20849–20857

52 Liu X, Ji Q, Hu Q, et al. Dual-mode long-lived luminescence of Mn^{2+}-doped nanoparticles for multilevel anticounterfeiting. ACS Appl Mater Interfaces, 2019, 11: 30146–30153

53 Zhou B, Yan L, Tao L, et al. Enabling photon upconversion and precise control of donor-acceptor interaction through interfacial energy transfer. Adv Sci, 2018, 5: 1700667

54 Zhu Q, Sun T, Chung M N, et al. Yb^{3+}-sensitized upconversion and downshifting luminescence in Nd^{3+} ions through energy migration. Dalton Trans, 2018, 47: 8581–8584

55 Chen X, Jin L, Sun T, et al. Energy migration upconversion in Ce(III)-doped heterogeneous core-shell-shell nanoparticles. Small, 2017, 13: 1701479

56 Deng R, Wang J, Chen R, et al. Enabling Förster resonance energy transfer from large nanocrystals through energy migration. J Am Chem Soc, 2016, 138: 15972–15979

57 Zhou B, Tao L, Chai Y, et al. Constructing interfacial energy transfer for photon up- and down-conversion from lanthanides in a core-shell nanostructure. Angew Chem Int Ed, 2016, 55: 12356–12360

58 Wen S, Zhou J, Zheng K, et al. Advances in highly doped upconversion nanoparticles. Nat Commun, 2018, 9: 2415

59 Siefe C, Mehlenbacher R D, Peng C S, et al. Sub-20 nm core-shell-shell nanoparticles for bright upconversion and enhanced Förster resonant energy transfer. J Am Chem Soc, 2019, 141: 16997–17005

60 Li Z, Park W, Zorzetto G, et al. Synthesis protocols for δ-doped $NaYF_4$:Yb,Er. Chem Mater, 2014, 26: 1770–1778

61 Chen X, Jin L, Kong W, et al. Confining energy migration in upconversion nanoparticles towards deep ultraviolet lasing. Nat Commun, 2016, 7: 10304

62 Lin X, Chen X, Zhang W, et al. Core-shell-shell upconversion nanoparticles with enhanced emission for wireless optogenetic inhibition. Nano Lett, 2018, 18: 948–956

63 Song X, Zhang J, Yue Z, et al. Dual-activator codoped upconversion nanoprobe with core-multishell structure for *in vitro* and *in vivo* detection of hydroxyl radical. Anal Chem, 2017, 89: 11021–11026

64 Song X, Yue Z, Zhang J, et al. Multicolor upconversion nanoprobes based on a dual luminescence resonance energy transfer assay for simultaneous detection and bioimaging of $[Ca^{2+}]_i$ and pH_i in living cells. Chem Eur J, 2018, 24: 6458–6463

65 Chen B, Liu Y, Xiao Y, et al. Amplifying excitation-power sensitivity of photon upconversion in a $NaYbF_4$:Ho nanostructure for direct visualization of electromagnetic hotspots. J Phys Chem Lett, 2016, 7: 4916–4921

66 Huang Z, Gao H, Mao Y. Understanding the effect of Mn^{2+} on Yb^{3+}/Er^{3+} upconversion and obtaining a maximum upconversion fluorescence enhancement in inert-core/active-shell/inert-shell structures. RSC Adv, 2016, 6: 83321–83327

67 Wang D, Xue B, Song J, et al. Compressed energy transfer distance for remarkable enhancement of the luminescence of Nd^{3+}-sensitized upconversion nanoparticles. J Mater Chem C, 2018, 6: 6597–6604

68 Liu Q, Zhang Y, Peng C S, et al. Single upconversion nanoparticle imaging at sub-10 W cm^{-2} irradiance. Nat Photon, 2018, 12: 548–553

69 Shen J W, Lu J, Tu J, et al. Enhanced 808 nm driven Ce^{3+} doped red-emitting upconversion nanocrystals by intercalated nanostructures. J Mater Chem C, 2016, 4: 4905–4911

70 Ding M, Chen D, Ma D, et al. Highly enhanced upconversion luminescence in lanthanide-doped active-core/luminescent-shell/active-shell nanoarchitectures. J Mater Chem C, 2016, 4: 2432–2437

71 Ma C, Xu X, Wang F, et al. Optimal sensitizer concentration in single upconversion nanocrystals. Nano Lett, 2017, 17: 2858–2864

72 Li D, Wen S, Kong M, et al. Highly doped upconversion nanoparticles for *in vivo* applications under mild excitation power. Anal Chem, 2020, 92: 10913–10919

73 Zhou B, Tang B, Zhang C, et al. Enhancing multiphoton upconversion through interfacial energy transfer in multilayered nanoparticles. Nat Commun, 2020, 11: 1174

74 Zhong Y, Tian G, Gu Z, et al. Elimination of photon quenching by a transition layer to fabricate a quenching-shield sandwich structure for 800 nm excited upconversion luminescence of Nd^{3+}-sensitized nanoparticles. Adv Mater, 2014, 26: 2831–2837

75 Choi J E, Kim D, Jang H S. Intense upconversion red emission from Gd-doped $NaErF_4$:Tm-based core/shell/shell nanocrystals under 980 and 800 nm near infrared light excitations. Chem Commun, 2019, 55: 2261–2264

76 Wang T, Zhou H, Yu Z, et al. 808 nm excited multicolor upconversion tuning through energy migration in core-shell-shell nanoarchitecture. J Phys Chem C, 2018, 122: 10113–10124

77 Guo S, Tsang M K, Lo W S, et al. 808 nm excited energy migration upconversion nanoparticles driven by a Nd^{3+}-trinity system with color-tunability and superior luminescence properties. Nanoscale, 2018, 10: 2790–2803

78 Lin S L, Chang C A. Optimising FRET-efficiency of Nd^{3+}-sensitised upconversion nanocomposites by shortening the emitter-photosensitizer distance. Nanoscale, 2020, 12: 8742–8749

79 Li Y, Zhang P, Ning H, et al. Emitting/sensitizing ions spatially separated lanthanide nanocrystals for visualizing tumors simultaneously through up- and down-conversion near-infrared Ⅱ luminescence *in vivo*. Small, 2019, 15: e1905344

80 Zhang Y, Zhang W, Zeng K, et al. Upconversion nanoparticles-based multiplex protein activation to neuron ablation for locomotion regulation. Small, 2020, 16: e1906797

81 Zhong Y, Rostami I, Wang Z, et al. Energy migration engineering of bright rare-earth upconversion nanoparticles for excitation by light-emitting diodes. Adv Mater, 2015, 27: 6418–6422

82 Baride A, May P S Jr, Berry M T. Cross-relaxation from $Er^{3+}(^2H_{11/2},^4S_{3/2})$ and $Er^{3+}(^2H_{9/2})$ in β-$NaYF_4$:Yb,Er and implications for modeling

upconversion dynamics. J Phys Chem C, 2019, 124: 2193–2201
83 Rabie H, Zhang Y, Pasquale N, et al. NIR biosensing of neurotransmitters in stem cell-derived neural interface using advanced core-shell upconversion nanoparticles. Adv Mater, 2019, 31: e1806991
84 Mizuno T, Hase E, Minamikawa T, et al. Full-field fluorescence lifetime dual-comb microscopy using spectral mapping and frequency multiplexing of dual-comb optical beats. Sci Adv, 2021, 7: eabd2102
85 Liu X, Lin D, Becker W, et al. Fast fluorescence lifetime imaging techniques: A review on challenge and development. J Innov Opt Health Sci, 2019, 12: 1930003
86 Suhling K, Hirvonen L M, Becker W, et al. Wide-field time-correlated single photon counting-based fluorescence lifetime imaging microscopy. Nucl Instrum Methods Phys Res Sect A-Accel Spectrom Dect Assoc Equip, 2019, 942: 162365
87 Liu X, Wang Y, Li X, et al. Binary temporal upconversion codes of Mn^{2+}-activated nanoparticles for multilevel anti-counterfeiting. Nat Commun, 2017, 8: 899
88 Fan Y, Wang P, Lu Y, et al. Lifetime-engineered NIR-II nanoparticles unlock multiplexed *in vivo* imaging. Nat Nanotechnol, 2018, 13: 941–946
89 Li H, Tan M, Wang X, et al. Temporal multiplexed *in vivo* upconversion imaging. J Am Chem Soc, 2020, 142: 2023–2030
90 Tan M, Li F, Wang X, et al. Temporal multilevel luminescence anticounterfeiting through scattering media. ACS Nano, 2020, 14: 6532–6538
91 Zhou L, Fan Y, Wang R, et al. High-capacity upconversion wavelength and lifetime binary encoding for multiplexed biodetection. Angew Chem Int Ed, 2018, 57: 12824–12829
92 Dong H, Sun L D, Feng W, et al. Versatile spectral and lifetime multiplexing nanoplatform with excitation orthogonalized upconversion luminescence. ACS Nano, 2017, 11: 3289–3297
93 Steiner S, Wolf J, Glatzel S, et al. Organic synthesis in a modular robotic system driven by a chemical programming language. Science, 2019, 363: eaav2211
94 Coley C W, Thomas III D A, Lummiss J A M, et al. A robotic platform for flow synthesis of organic compounds informed by AI planning. Science, 2019, 365: eaax1566
95 Mehr S H M, Craven M, Leonov A I, et al. A universal system for digitization and automatic execution of the chemical synthesis literature. Science, 2020, 370: 101–108

Summary for “多层结构对镧系掺杂纳米颗粒上转换发光的调控作用”

Regulating the upconversion luminescence of lanthanide-doped nanoparticles through multilayered structure

Changyun Qin, Xianbin Xie & Ying Ma*

State Key Laboratory of Materials Processing and Die & Mould Technology, School of Materials Science and Engineering, Huazhong University of Science and Technology, Wuhan 430074, China
* Corresponding author, E-mail: yingma@hust.edu.cn

The concept of upconversion luminescence (UCL) was first proposed by Bloembergen in 1959. As a nonlinear optical process, photon upconversion in lanthanide-doped upconversion nanoparticles (UCNPs) features by sequential absorption of multiple low-energy photons via the long-lived intermediate energy states of lanthanide ions and emission of high-energy photons. Unlike common luminescent materials such as organic dyes and quantum dots, lanthanide-doped UCNPs exhibit large anti-Stokes shift, excellent stability against photobleaching, long fluorescence lifetime and sharp multiline emissions, enabling a variety of applications, such as bioimaging, anti-counterfeiting, diagnosis, photodynamic therapy, background-free biosensing, solar energy harvesting and super-resolution nanoscopy. However, it is still challenging for these UCNPs to be utilized practically because of limited UCL brightness. Firstly, the UCL is severely quenched by surface quenchers like ligands and defects. Moreover, the cross-relaxation between lanthanide-doped ions suppresses upconversion efficiency to a large extent. What’s worse, the limited excitation light harvesting due to the parity-forbidden nature of 4f-4f electronic transitions still remains a hindrance for UCL enhancement.

Design of the core-shell (C/S) structure, via coating a protecting shell on the luminescent core, can significantly suppress the energy transfer from core to surface quenchers (defects, ligands, etc.) for lanthanide-doped UCNPs. Therefore, the C/S engineering of lanthanide-doped UCNPs can enhance UCL significantly and has been widely adopted and investigated since it was first proposed in 2007. Recently, multilayered structures have attracted more and more attention because these structures offer versatile modulation ways on their optical properties and make them highly potential for application.

In this review, we summarize the merits of these multilayered UCNPs and their practical applications in various fields. First of all, we introduce the flexible modulation on UCL performance via multilayered structure, such as full-color emissions and orthogonal excitations-emissions, which can be applied in full-color display and image-guided photodynamic therapy. Secondly, we emphasize the controllable energy upconversion and migration in multilayered UCNPs, enriching sensitizer-activator pairs with an efficient upconversion. Subsequently, we describe the significant enhancement in brightness and upconverting efficiency for heavily doped UCNPs via designing multilayered structure, with minimizing the energy loss and cross-relaxation. Last but not the least, we present the distinguished lifetime tunability of multilayered UCNPs, which are favorable for multiplexing, deep-tissue imaging and multi-level anti-counterfeiting.

The multilayered structures make it more possible for us to design and synthesize bright, versatile lanthanide-doped UCNPs to meet the demands of various applications. However, challenges still remain in practical utilization of these UCNPs. On the one hand, the absorption cross-section of lanthanide ions is relatively small for harvesting excitation light. Introduction of organic antenna, construction of photonic crystals and plasma enhancement by composition with metal nanostructures may also be applicable for these multilayered UCNPs. On the other hand, it is urgent to develop a simple and controllable method for constructing multilayered UCNPs. The great progress of artificial intelligence may be helpful for us to synthesize UCNPs with complex structures more easily and controllably.

upconversion nanoparticles, multilayered structure, energy transfer regulation, highly efficient luminescence, photoluminescence lifetime tunability

doi: 10.1360/TB-2020-1565